Interfacial compositions of solid and liquid in a phase-field model with finite interface thickness for isothermal solidification in binary alloys

Seong Gyoon Kim
RASOM and Department of Materials Science and Engineering, Kunsan National University, Kunsan 573-701, Korea

Won Tae Kim
RASOM and Department of Physics, Chongju University, Chongju 360-764, Korea

Toshio Suzuki
Department of Metallurgy, The University of Tokyo, Tokyo 113, Japan
(Received 10 December 1997)

We show that a finite interface thickness in an isothermal phase-field model for alloy solidification introduces a chemical potential gradient in the interfacial region and the solute trapping effect, and the relationships between material properties and parameters in the phase-field equation can be determined at a low interface velocity limit condition. Also we show that there are upper bounds on the interface thickness and the interface kinetics coefficient, which vary with thermophysical properties of alloys. The predicted compositions of solid and liquid at the interface with this model are in good agreement with those obtained by numerical simulation of one-dimensional isothermal solidification of an Al–2-mole-%-Si alloy at 870 K. [S1063-651X(98)01309-9]

PACS number(s): 64.70.Dv, 81.30.Fb, 81.10.Aj, 05.70.Ln

I. INTRODUCTION

Phase-field models are known to be very powerful in describing the complex pattern evolution of the interface between mother and new phases in a nonequilibrium state. Such models are efficient especially in numerical treatment because all the governing equations are written as unified equations in the whole space of the system without distinguishing the interface from the mother and the new phase, and direct tracking of the interface position is not needed during numerical calculation. Recently several phase-field models have been developed mainly for the solidification of pure materials [1–9] and they have been extended to the solidification of binary alloys with a single solid phase [10–13] or with two solid phases [14–17].

In the phase-field models developed for calculating interface morphology and solute redistribution during solidification of alloys, parameters in the phase-field equation can be described by material parameters with certain relationships. The relationships are normally derived by matching the asymptotic limit of the phase-field equation in zero interface thickness with the traditional sharp interface condition. In this case, with increasing interface velocity both solid and liquid composition at the interface, determined by a parallel tangent rule, become lower than equilibrium values [14]. However, there is much evidence showing that both solid and liquid compositions at interface approach each other in the bulk composition with increasing interface velocity [18]. The current theories on this phenomenon called solute trapping, are based on the finite relaxation time for equilibrium partitioning of the atoms at the interface [19,20]; with increasing interface velocity, time for the diffusion of atoms to relax into the equilibrium compositions becomes limited and solid and liquid compositions approach each other. A phase-field model describing solute trapping during solidification of alloys has been proposed by Wheeler, Boettinger, and McFadden [21,22]. In their model, the concentration gradient energy term, in addition to the phase-field gradient term, is included in the free energy functional. The model has been applied to the cases including the transient effect of solute profile [23] or thermal effect [24]. As pointed out in Ref. [25], however, the concentration gradient energy term is not a necessary condition for solute trapping. The finite interface thickness can result in the solute trapping effect, because the relaxation time for partitioning of the solute atoms in the diffuse interface should be finite in that case. In order to describe the solute trapping effect by a phase-field model without concentration gradient energy term, therefore, we need the parameters of the phase-field equation determined at a finite interface thickness condition, not at a sharp interface limit condition. Recently Karma and Rappel [26] have shown that it is really feasible to determine the parameters in the phase-field equation at the finite interface thickness condition for solidification of pure materials.

In this article we examine the effect of interface velocity on the compositions of solid and liquid at the interface in a phase-field model with a finite interface thickness for isothermal solidification of binary alloys. At first, at finite interface thickness condition, we will derive relationships between material properties such as interface thickness, the interface energy, and the parameters in the phase-field equation such as imposed double-well potential height and the coefficient of phase-field gradient energy. Next, at a low interface velocity limit condition, we will derive the chemical potentials of the solid and liquid phases at the interface and show that a finite interface thickness leads to the chemical potential gradient within the interfacial region and results in the solute trapping effect. And we will derive the relationship between linear interface kinetics coefficient and phase-field mobility. Finally using one-dimensional numerical simulation on isothermal solidification of an Al–2-mole-%-Si alloy, we will test the solute trapping behavior and

compare the compositions of solid and liquid at interface with those predicted at a low interface velocity limit condition.

II. GOVERNING EQUATIONS

The free energy density of a solid-liquid mixture may be written in the form

$$f(c,\phi)=h(\phi)f^S(c)+[1-h(\phi)]f^L(c)+wg(\phi), \quad (1)$$

where f^S and f^L are the free energy density of the solid and liquid phases, respectively, and functions of solute mole fraction c. The phase field ϕ is defined as a continuous variable between $\phi=1$ at solid and $\phi=0$ at liquid phase, and like Warren and Boettinger [12] we choose

$$h(\phi)=\phi^3(6\phi^2-15\phi+10) \quad (2)$$

and

$$wg(\phi)=w\phi^2(1-\phi)^2, \quad (3)$$

where $g(\phi)$ is the double-well potential associated with the phase change and w is the barrier height. Even though we take a constant w independent of composition, it does not necessarily imply that the interface energy is independent of the temperature, in the case with finite interface thickness. As will be shown in Sec. IV, the interface energy is dependent on detailed shapes of the free energy curves of solid and liquid phases and therefore varies with temperature and equilibrium interfacial concentration. We do not impose any restriction on the functional forms of the the free energy density of the solid and liquid phases, and any solution model or thermodynamic data for them may be adopted.

Time dependence of the phase field and concentration field, where positive local entropy production is guaranteed, can be described by [14]

$$\phi_t=M(\epsilon^2\nabla^2\phi-f_\phi) \quad (4)$$

and

$$c_t=\nabla\cdot\left(\frac{D(\phi)}{f_{cc}}\nabla f_c\right), \quad (5)$$

where t is time and M the mobility of the phase field. The ϵ in Eq. (4) and w in f are the parameters which are related with interfacial energy and interface thickness. $D(\phi)$ is the chemical diffusivity, which is a function of phase field. Equation (5) guarantees constant diffusivities in bulk solid and liquid, and mass balance at the interface in sharp interface limit, irrespective of the free energy density model. In this study we will consider only instantaneous steady state in one dimension. When an interface moves to positive x direction during solidification, the governing equations become

$$-v_n\frac{d\phi}{dx}=M\left(\epsilon^2\frac{d^2\phi}{dx^2}-f_\phi\right) \quad (6)$$

and

$$-v_n\frac{dc}{dx}=\frac{d}{dx}\left(\frac{D(\phi)}{f_{cc}}\frac{df_c}{dx}\right). \quad (7)$$

For a curved interface in non-steady-state, however, it can be shown that the rigorous asymptotic analysis gives the same key results as those in the one-dimensional steady-state case except for the presence of the curvature effect.

III. STATIONARY SOLUTIONS

At thermodynamic equilibrium state, the concentration $c_0(x)$ and phase field $\phi_0(x)$ are determined by

$$f_c(c_0(x),\phi_0(x))=f_c^e(\text{const}) \quad (8)$$

and

$$\epsilon^2\frac{d^2\phi_0}{dx^2}=f_\phi(c_0,\phi_0), \quad (9)$$

where f_c^e is the chemical potential at a thermodynamic equilibrium state to be found from the phase-field equation. Equation (8) can be rewritten as

$$f_{cc}(c_0,\phi_0)dc_0+f_{c\phi}(c_0,\phi_0)d\phi_0=0. \quad (10)$$

If free energy density $f(c,\phi)$ for an alloy is given, stationary concentration profiles as a function of ϕ_0,

$$c_0(x)=\tilde{c}(\phi_0(x)), \quad (11)$$

can be found by numerical method in general under the boundary conditions of $c_0=c_S^e$ at $\phi_0=1$ and $c_0=c_L^e$ at $\phi_0=0$, where c_L^e and c_S^e are equilibrium compositions of liquid and solid, respectively, at a given temperature. If we define a function F as

$$F(c,\phi)=f(c,\phi)-f_c^e c, \quad (12)$$

then $f_\phi(c_0,\phi_0)=dF(c_0,\phi_0)/d\phi$ because $F_c(c_0,\phi_0)=0$ by Eq. (8), and then Eq. (9) may be modified into

$$\epsilon^2\frac{d^2\phi_0}{dx^2}=\frac{dF(\tilde{c}_0(\phi_0),\phi_0)}{d\phi_0}. \quad (13)$$

Integrating this equation after multiplying $d\phi_0/dx$ on both sides results in

$$\frac{d\phi_0}{dx}=-\frac{\sqrt{2}}{\epsilon}\sqrt{F(\phi_0)-F(0)}. \quad (14)$$

Integration of this equation yields $\phi_0(x)$ if the relevant thermodynamic data for an alloy and w and ϵ are given. Because $\phi_0=1$ in bulk solid, this equation gives $F(1)=F(0)$, and we get the equilibrium chemical potential

$$f_c^e=\frac{f^L(c_L^e)-f^S(c_S^e)}{c_L^e-c_S^e}. \quad (15)$$

The function $F(\phi_0)-F(0)$ can be expressed as the sum of two potentials;

$$F(\phi_0)-F(0)=w\phi_0^2(1-\phi_0)^2+[Z(\phi_0)-Z(0)], \quad (16)$$

where the function $Z(\phi_0)$ is defined by

$$Z(\phi_0) \equiv h(\phi_0) f^S(\tilde{c}(\phi_0)) + [1-h(\phi_0)] f^L(\tilde{c}(\phi_0)) - f_c^e \tilde{c}(\phi_0). \quad (17)$$

When the free energy curves of both solid and liquid phases are convex downward against composition, we can see that $Z(0)=Z(1)$, $Z(\phi_0) \geqslant Z(0)$, and the $Z(\phi_0)-Z(0)$ has a positive maximum value near the position of $f^S(\tilde{c}(\phi_0)) = f^L(\tilde{c}(\phi_0))$, as long as the $\tilde{c}(\phi_0)$ decreases monotonically with ϕ_0. Therefore Eq. (16) is composed of two double-well potentials. The height of the first potential must be controlled to be matched with interface energy and interface thickness. On the other hand, the second potential is a fixed one for an isothermal system, which is given by definition of free energy for the interfacial region. The existence of the $Z(\phi_0)-Z(0)$ imposes a restriction on the interface thickness, as will be shown in the next section.

IV. PARAMETERS IN THE PHASE-FIELD EQUATION

The parameters ϵ, w, and M in the phase-field equation are to be matched with the interface energy σ, interface thickness 2λ, and interface kinetics coefficient μ_k. In this section the parameters ϵ and w are found from σ and 2λ with a finite interface thickness condition, not with sharp interface limit condition, and the relationship between M and μ_k will be found in the next section.

When the concentration gradient energy term is not included as in this study, interface energy at equilibrium state is given by [21]

$$\sigma = \epsilon^2 \int_{-\infty}^{+\infty} \left(\frac{d\phi_0}{dx} \right)^2 dx. \quad (18)$$

Using Eq. (14), this may be rewritten as

$$\sigma = \sqrt{2}\epsilon \int_0^1 \sqrt{F(\phi_0)-F(0)}\, d\phi_0. \quad (19)$$

Equation (14) also gives a measure of the interface thickness, over which the phase field changes from 0.1 to 0.9;

$$2\lambda = \frac{\epsilon}{\sqrt{2}} \int_{0.1}^{0.9} \frac{d\phi_0}{\sqrt{F(\phi_0)-F(0)}}. \quad (20)$$

Two parameters ϵ and w in the phase-field equation can be determined by numerical integration of Eqs. (19) and (20) for a fixed interface energy and thickness. These relationships are dependent on the system temperature because $Z(\phi_0)-Z(0)$ term is a function of temperature. Also notice that the $Z(\phi_0)-Z(0)$ term limits both interface thickness and the interfacial energy as follows:

$$2\lambda \leqslant \frac{\epsilon}{\sqrt{2}} \int_{0.1}^{0.9} \frac{d\phi_0}{\sqrt{Z(\phi_0)-Z(0)}} \quad (21)$$

and

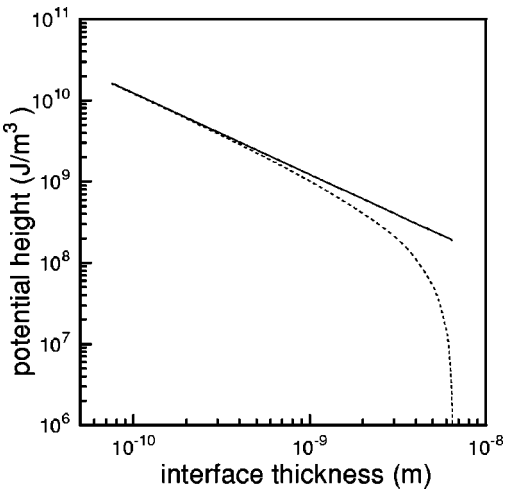

FIG. 1. Variations of the height of the double-well potential w with interface thickness: calculated with a finite interface thickness condition (dotted line) and with sharp interface limit condition (solid line) for Al–2-mole-%-Si alloy at 870 K with an interfacial energy of 0.093 J/m^2.

$$\sigma \geqslant \sqrt{2}\epsilon \int_0^1 \sqrt{Z(\phi_0)-Z(0)}\, d\phi. \quad (22)$$

Combining the above two inequalities yields

$$2\lambda \leqslant \frac{\sigma}{2} \frac{\int_{0.1}^{0.9} [1/\sqrt{Z(\phi_0)-Z(0)}]\, d\phi_0}{\int_0^1 \sqrt{Z(\phi_0)-Z(0)}\, d\phi_0}. \quad (23)$$

This limiting condition on the interface thickness may cause a serious problem in numerical applications. For example, Eq. (23) gives a condition that $2\lambda \leqslant 6.51$ nm in the Al–2-mole-%-Si alloy system at 870 K when thermophysical data are used. This seems to be a serious grid size limitation in numerical approach, especially in a two-dimensional simulation, on the phase-field modeling for alloy solidification. If we select a sufficiently thin interface while keeping a fixed solid-liquid interfacial energy, ϵ should be very small and w very large. In this situation, the second potential in Eq. (16) can be negligible compared with the first potential well, and the solution of Eq. (14) is given by

$$\phi_0(x) = \frac{1}{2}\left[1 - \tanh\left(\frac{\sqrt{w}}{\epsilon\sqrt{2}}\, x \right) \right], \quad (24)$$

and then Eqs. (19) and (20) yield

$$2\lambda \simeq 2.2\sqrt{2}\, \frac{\epsilon}{\sqrt{w}} \quad (25)$$

and

$$\sigma = \frac{\epsilon\sqrt{w}}{3\sqrt{2}}, \quad (26)$$

which are just the same parameter relationships as for pure materials in the sharp interface limit [5]. Figure 1 shows variations of the height of the double-well potential w ob-

TABLE I. Thermophysical data for dilute Al-Si alloy.

D_S (m^2/s)	1×10^{-12}
D_L (m^2/s)	3×10^{-9}
T_M (K)	933.6
V_m (m^3/mole)	1.06×10^{-5}
σ (J/m^2)	0.093
$f^S V_m$ (J/mole)[a]	$G^0_{Al}(1-c)+G^0_{Si}c+RT[c\ \ln c+(1-c)\ln(1-c)]+A^S c(1-c)$
$f^L V_m$ (J/mole)[a]	$RT[c\ \ln c+(1-c)\ln(1-c)]+c(1-c)[A^L+B^L(1-2c)+C^L(1-6c+6c^2)]$
G^0_{Al} (J/mole)[a]	$-10792+11.56T$
G^0_{Si} (J/mole)[a]	$12.12T$
A^S (J/mole)[a]	$-200-7.594T$
A^L (J/mole)[a]	$-10695.4-1.823T$
B^L (J/mole)[a]	$-4274.5-3.044T$
C^L (J/mole)[a]	$670.7-0.460T$
c^e_S	0.006387 (at 870 K)
c^e_L	0.07919 (at 870 K)
k^e	0.0807 (at 870 K)
m^e (K)	939.0 (at 870 K)

[a]Data from Ref. [27].

tained by numerical integration of Eqs. (19) and (20) (dotted line) and by Eqs. (25) and (26) (solid line) for an Al–2-mole-%-Si alloy at 870 K with interfacial energy of 0.093 J/m^2 and thermophysical data given in Table I. In this figure it is clear that w obtained from a finite interface thickness condition deviates significantly from that from the sharp interface limit condition when the interface thickness is larger than about 1 nm. This indicates that parameter relationships obtained with the sharp interface limit condition may be used for numerical simulation only with a very restrictive interface thickness. If we use Eqs. (19) and (20) to determine w and ϵ values, on the other hand, we may increase the interface thickness. However, there is still a limit on the interface thickness given by inequality (23). When $w=0$, the calculated interface thickness limit is 6.51 nm for the Al–2-mole-%-Si alloy. If we enforce the interface thickness to be over the limit in numerical simulation, it leads inevitably to an increased interfacial energy. The ϵ value obtained from Eqs. (19) and (20) was very close to that with the sharp interface limit condition in the whole range of interface thickness in Fig. 1. The difference in ϵ values determined by the two different methods was less than 2%.

V. LOW INTERFACE VELOCITY LIMIT

In this section we seek chemical potentials and compositions at solid and liquid sides of the diffuse interface with a low interface velocity limit to find a relationship between interface kinetics coefficient and parameters in the phase-field equation.

We integrate Eq. (7) to yield

$$v_n c(x)+\frac{D(\phi)}{f_{cc}}\frac{df_c}{dx}=A, \tag{27}$$

where A is an integration constant. In liquid and solid sides of the interface, Eq. (27) gives $D_L dc_L/dx=A-v_n c_L$ and $D_S dc_S/dx=A-v_n c_S$, where c_S and c_L are the compositions at solid and liquid sides of the interface, respectively. Eliminating the constant A, we get the well-known mass-conservation condition at interface.

Now we assume that the diffusivity in solid phase D_S is so small that the diffusion boundary layer outside of the interfacial layer is negligible. This assumption is reasonable in most cases of rapid solidification where the phase-field model can be used as a powerful tool in numerical simulation of pattern formation. Under this assumption the constant A in Eq. (27) becomes $v_n c_S$ because the concentration gradient in the solid is zero. The chemical potential profile therefore is given by

$$f_c(x)=f^S_c(c_S)-v_n\int_{-\infty}^{x}\frac{f_{cc}}{D(\phi)}[c(x)-c_S]dx, \tag{28}$$

where $f^S_c(c_S)$ is an integration constant which is just the chemical potential of the solid phase. Although interface velocity dependent concentration profile $c(x)$ may be found, it is not relevant to the analysis at low interface velocity. The composition c_L and chemical potential $f^L_c(c_L)$ at the liquid side of the interface are not clearly defined because of the diffuseness of the phase change in the phase-field model. As a first approximation, we simply assume that the thermodynamic partitioning of concentration at the interface occurs sufficiently over the width of $-\lambda<x<\lambda$. This assumption will be tested in Sec. VI. The chemical potential $f^L_c(c_L)$ then is given by

$$f^L_c(c_L)\simeq f^S_c(c_S)-v_n\int_{-\lambda}^{\lambda}\frac{f_{cc}}{D(\phi)}[c(x)-c_S]dx. \tag{29}$$

The chemical potential of the solid is determined by the phase-field equation. Integrating from $x=-\lambda$ to $x=\lambda$ after multiplying $d\phi/dx$ on both sides of Eq. (6), we get

$$-\frac{v_n}{M}\int_{-\lambda}^{\lambda}\left(\frac{d\phi}{dx}\right)^2 dx=\epsilon^2\int_{-\lambda}^{\lambda}\frac{d^2\phi}{dx^2}\frac{d\phi}{dx}dx-\int_{-\lambda}^{\lambda}\frac{\partial f}{\partial\phi}\frac{d\phi}{dx}dx. \tag{30}$$

By Eq. (28), the last term on the right-hand side of Eq. (30) becomes

$$\int_{x=-\lambda}^{x=\lambda}\frac{\partial f}{\partial\phi}d\phi=f^L(c_L)-f^S(c_S)-f^S_c(c_S)(c_L-c_S)+v_n\int_{c_S}^{c_L}\left(\int_{-\lambda}^{x}\frac{f_{cc}}{D(\phi)}[c(x')-c_S]dx'\right)dc. \tag{31}$$

Equation (30) therefore can be written as

$$f^L(c_L)-f^S(c_S)-f^L_c(c_L)(c_L-c_S)=v_n\left[\frac{1}{M}\int_{-\infty}^{\infty}\left(\frac{d\phi}{dx}\right)^2 dx+\int_{c_S}^{c_L}\left(\int_{x}^{\lambda}\frac{f_{cc}}{D(\phi)}[c(x')-c_S]dx\right)dc\right], \tag{32}$$

where we took $\lambda \to \infty$ at the first terms in both sides of Eq. (30) and replaced f_c^S in Eq. (31) by f_c^L given by Eq. (29).

Now we consider a situation when the interface velocity is low. In this case the first-order equations in v_n corresponding to Eqs. (29) and (32) become

$$f_c^L(c_L) = f_c^S(c_S) - \beta v_n \tag{33}$$

and

$$f^L(c_L) - f^S(c_S) - f_c^L(c_L)(c_L - c_S) = \alpha v_n, \tag{34}$$

where α and β are the constants for a given temperature and are defined as follows:

$$\beta = \int_{-\lambda}^{\lambda} \frac{f_{cc}(c_0, \phi_0)}{D(\phi_0)} [c_0(x) - c_S^e] dx \tag{35}$$

and

$$\alpha = \frac{1}{M} \int_{-\infty}^{\infty} \left(\frac{d\phi_0}{dx} \right)^2 dx + \int_{c_S^e}^{c_L^e} \left(\int_x^{\lambda} \frac{f_{cc}(c_0, \phi_0)}{D(\phi_0)} \times [c_0(x') - c_S^e] dx' \right) dc_0, \tag{36}$$

where $c_0(x)$ and $\phi_0(x)$ are stationary concentration and phase fields, respectively, which are the solutions of Eqs. (10) and (14). The α and β may be modified into more tractable forms by using Eqs. (10), (14), and (18) as follows:

$$\beta = \frac{\epsilon}{\sqrt{2}} \int_{0.1}^{0.9} \frac{f_{cc}(\tilde{c}_0, \phi_0)}{D(\phi_0)\sqrt{F(\phi_0) - F(0)}} [\tilde{c}_0(\phi_0) - c_S^e] d\phi_0 \tag{37}$$

and

$$\alpha = \frac{\sigma}{M\epsilon^2} + \frac{\epsilon}{\sqrt{2}} \int_{0.1}^{0.9} \left(\int_{0.1}^{\phi_0} \frac{f_{cc}(\tilde{c}_0, \phi_0')}{D(\phi_0')\sqrt{F(\phi_0') - F(0)}} \times [\tilde{c}_0(\phi_0') - c_S^e] d\phi_0' \right) \frac{f_{c\phi}(\tilde{c}_0, \phi_0)}{f_{cc}(\tilde{c}_0, \phi_0)} d\phi_0. \tag{38}$$

Two coupled equations (33) and (34) determine chemical potentials and compositions at solid and liquid sides of the diffuse interface as functions of interface velocity.

In Eqs. (33) and (34), some interesting limiting cases are included. first, with sharp interface limit condition and infinite phase-field mobility M, we can obtain the following relationship because $\lambda \to 0$, $\alpha \to 0$, and $\beta \to 0$ in this limit condition:

$$f_c^L(c_L) = f_c^S(c_S) = \frac{f^L(c_L) - f^S(c_S)}{c_L - c_S}, \tag{39}$$

which can be interpreted as the common tangent rule for the local equilibrium condition at the interface. Secondly, with the sharp interface limit condition and a finite phase-field mobility, the following relationship can be obtained:

$$f_c^L(c_L) = \tilde{f}_c^S(c_S) = \frac{f^L(c_L) - \tilde{f}^S(c_S)}{c_L - c_S}, \tag{40}$$

where

$$\tilde{f}^S(c_S) = f^S(c_S) + \frac{v_n}{M} \int_{-\infty}^{\infty} \left(\frac{d\phi_0}{dx} \right)^2 dx. \tag{41}$$

This means that c_S and c_L are determined by a common tangent rule with a correction on the free energy density of the solid, which may be interpreted as a parallel tangent rule named by Wheeler, Boettinger, and McFadden [10]. As reported by them, the finite phase-field mobility causes both c_S and c_L to decrease with increasing interface velocity in this limiting case. Thirdly, with a finite interface thickness and infinite phase-field mobility, we can obtain the chemical potentials of solid and liquid sides at the interface as follows:

$$f_c^S(c_S) = \frac{f^L(c_L) - f^S(c_S)}{c_L - c_S} + \frac{v_n}{c_L - c_S} \int_{c_S^e}^{c_L^e} \left(\int_{-\lambda}^{x} \frac{f_{cc}(c_0, \phi_0)}{D(\phi_0)} \times [c_0(x') - c_S^e] dx' \right) dc \tag{42}$$

and

$$f_c^L(c_L) = \frac{f^L(c_L) - f^S(c_S)}{c_L - c_S} - \frac{v_n}{c_L - c_S} \int_{c_S^e}^{c_L^e} \left(\int_x^{\lambda} \frac{f_{cc}(c_0, \phi_0)}{D(\phi_0)} \times [c_0(x') - c_S^e] dx' \right) dc. \tag{43}$$

In an alloy system with the free energy curves of solid and liquid phases convex downward against composition and with negative liquidus and solidus slopes in the phase diagram, f_{cc} is always positive and c_L is larger than c_S. In this case, as long as the stationary composition $c_0(x)$ in the interfacial region is between c_S^e and c_L^e, we can get the inequalities

$$f_c^S(c_S) \geqslant \frac{f^L(c_L) - f^S(c_S)}{c_L - c_S} \tag{44}$$

and

$$f_c^L(c_L) \leqslant \frac{f^L(c_L) - f^S(c_S)}{c_L - c_S}. \tag{45}$$

Note that these inequalities can hold only when $c_S \geqslant c_S^e$ and $c_L \leqslant c_L^e$, indicating that the compositions on the solid and liquid sides of the interface approach each other with increasing interface velocity. From Eqs. (42) and (43), for a given alloy at a constant temperature, we see that the chemical potentials (and also the compositions) of solid and liquid at interface are governed by the interfacial Péclet number which is defined by $\mathrm{Pe} = 2\lambda v_n / \tilde{D}$ where $\tilde{D}$ is the average diffusivity at the interface. This behavior of the interfacial composition, known as the solute trapping phenomenon [18], is the natural result. With increasing interface velocity, time for the diffusion of atoms to relax into the equilibrium com-

positions decreases and the difference between solid and liquid compositions at the interface should decrease. The relative scale of the interface velocity v_n to the relaxation speed of the atom at the interface can be estimated as the interfacial Péclet number. The interfacial Péclet number thus plays a key role in solute trapping. When both the interface thickness and phase-field mobility are finite, c_L decreases with increasing interface velocity because they both cause c_L to decrease. However, with increasing interface velocity, c_S can decrease or increase depending on the relative magnitude of two terms on the right-hand side of Eq. (36).

Considering that the left-hand side term in Eq. (34) is the thermodynamic driving force for the formation of the solid with composition c_S from the liquid with composition c_L [28], it is clear that the interface velocity is linear with the driving force. For a dilute solution, following Boettinger and Coriell [29], Eq. (34) can be modified into

$$T=T_M-m^e c_L\left(1+\frac{(k^e-k)+k\ \ln(k/k^e)}{(1-k^e)}\right)-\frac{V_m}{RT}\frac{\alpha m^e}{1-k^e}v_n, \tag{46}$$

where T is the temperature of the isothermal system, and T_M is the equilibrium melting temperature of pure solvent, m^e is the equilibrium liquidus slope in phase diagram, V_m is molar volume, R is the gas constant, $k=c_S/c_L$, and $k^e=c_S^e/c_L^e$. The second and third terms on the right-hand side of Eq. (46) are the constitutional undercooling with a nonequilibrium correction and kinetics undercooling, respectively. According to the conventional definition of the interface kinetics coefficient μ_k [18], we then obtain

$$\mu_k=\frac{RT}{V_m}\frac{1-k^e}{\alpha m^e}, \tag{47}$$

where α is given by Eq. (38). Thus all the parameters ϵ, w, and M in the isothermal phase-field model with a finite interface thickness can be determined by using Eqs. (19), (20), (38), and (47) if interface energy, interface thickness, interface kinetics coefficient, and free energy densities of solid and liquid as functions of composition are given. Even when phase-field mobility is infinite, the interface kinetics coefficient must be a finite value due to the second term on the right-hand side of Eq. (38), as long as the interface thickness is nonzero, that is, $\epsilon\neq 0$. The finite interface thickness therefore imposes a limit on μ_k. For the Al–2-mole-%-Si alloy at 870 K, for example, by using Eqs. (38) and (47) it can be shown that the interface thickness of 3 nm yields the maximum μ_k of 0.0195 m/s K when M is infinite.

VI. NUMERICAL SIMULATION

In this section the steady-state concentrations of solid and liquid at the interface obtained by numerical analysis for one-dimensional isothermal solidification were compared with those predicted by Eqs. (33) and (34) under the low interface velocity limit condition.

The steady state can be obtained by solving directly steady-state equations for a given temperature, or solving non-steady-state equations with the proper boundary conditions under which the steady state is guaranteed at long time behavior. We relied on the latter method. The initial condition of our system is an undercooled state with a given system temperature, and then a solid phase with the same composition as the bulk liquid nucleates and starts to grow freely. As time goes on, due to solute pile-up in the liquid phase, the interface velocity decreases monotonically and finally stops at an equilibrium state. Thus there is no steady state in this one-dimensional (1D) free-growth system. In order to get a steady state, therefore, we should impose some conditions on our system. If total solute mass is to be conserved, the condition should be that the far-field concentration in solid ($c_s^{-\infty}$) is the same as that in liquid ($c_s^{+\infty}$). In this case we can get a unique steady-state interface velocity for a given temperature and a bulk composition. If mass is not to be conserved, however, it is possible to impose a different condition to get steady state; suppose an imaginary solute sink in liquid, moving with the same instantaneous velocity as the interface, maintaining a prescribed distance from the moving interface. If the solute sink engulfs all solute influx from its neighbor, the steady state can exist at long time behavior even when $c_s^{-\infty}$ is different from $c_s^{+\infty}$ because the system has an additional degree of freedom (the distance between solute sink and interface). In this case the interface velocity is not uniquely dependent on the system temperature and bulk composition, but should depend on the imposed distance between sink and interface. With this technique we will check the effect of interface velocity on the interfacial compositions of solid and liquid at a given temperature. Note that our parameters depending only on the system temperature in the phase-field equation do not depend on the bulk composition.

The Al–2-mole-%-Si alloy was selected as a model system and all calculations were performed at 870 K with thermophysical data given in Table I. The interface thickness 2λ was taken as 3 nm, and the grid size of 0.5 nm was used so that the interfacial region ranges over six grid spacing. The total grid number was fixed to be 1500. With the interface thickness of 3 nm and the interface energy $\sigma=0.093$ J/m^2, the parameters w and ϵ obtained from Eqs. (19) and (20) were 2.10×10^8 J/m^3 and 1.91×10^{-5} (J/m)$^{1/2}$, respectively. The phase-field mobility M was treated as a variable to observe its effect on the compositions of solid and liquid at interface. By using Eqs. (38) and (47), of course, one may evaluate the corresponding interface kinetics coefficient μ_k under assumption of dilute solution of mixture.

Equations (4) and (5) were discretized by a second-order differencing scheme for spatial derivatives and a simple explicit Euler scheme for time derivative, conserving the total mass. The $f_{cc}/D(\phi)$ at the boundary between the ith and the $(i+1)$th grid was determined by

$$\left(\frac{D(\phi)}{f_{cc}(c,\phi)}\right)^{i+1/2}=\frac{D(\phi^{i+1/2})}{f_{cc}(c^{i+1/2},\phi^{i+1/2})}, \tag{48}$$

where the concentration $c^{i+1/2}$ and phase field $\phi^{i+1/2}$ at grid boundary were obtained by Lagrange interpolation on four neighboring grid points. The dependence of diffusivity on ϕ was assumed as

$$D(\phi)=h(\phi)D_S+[1-h(\phi)]D_L, \tag{49}$$

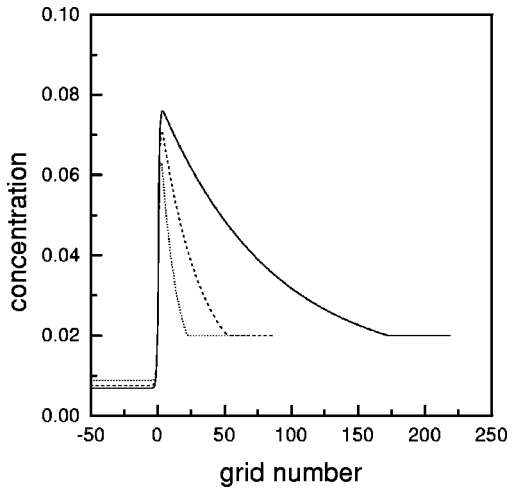

FIG. 2. Steady-state concentration profiles calculated with $M=44$ m^3/J s for Al–2-mole-%-Si alloy at 870 K. The origin was taken as the position with $\phi=0.5$. The interface velocities are 0.060 m/s for solid line, 0.20 m/s for dashed line, and 0.50 m/s for dotted line.

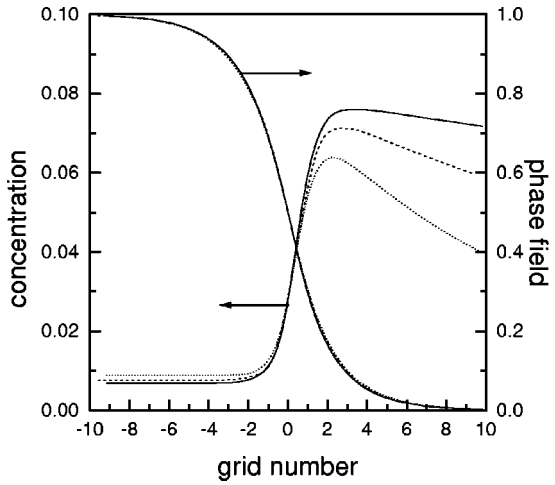

FIG. 3. The detailed phase-field and concentration profiles around the interface, corresponding to Fig. 2.

where D_S and D_L are the diffusivities in bulk solid and liquid, respectively. Initial liquid composition was uniform with 2.0 silicon mole % and the system temperature in all simulations was fixed to be 870 K. Solidification started after seeding of a small solid with the same composition with the liquid at one end of the system. In order to guarantee existence of steady state at long time behavior, we put a moving solute sink in liquid, maintaining a prescribed distance from the interface. In every time step, the solute sink was moved by just the interface migration distance and enforced to maintain the initial bulk composition. The system reached a steady state after a transient period. The interface velocity at the steady state could be varied by changing the prescribed distance between solute sink and interface.

Figure 2 shows steady-state concentration profiles with $M=44$ m^3/J s and three different fixed distances, where the origin was taken as the position of $\phi=0.5$. The position of the solute sink can be seen in each profile, where the composition in liquid abruptly goes to the initial bulk composition. The measured interface velocities were 0.060 m/s (solid line), 0.20 m/s (dashed line), and 0.50 m/s (dotted line) for three different prescribed distances between solute sink and interface. Note that the maximum and the minimum concentrations approach each other with increasing interface velocity. The detailed corresponding phase field and concentration profiles around the interface are shown in Fig. 3. In this figure, interface thickness over which phase field changes from 0.1 to 0.9 is just six grid spacing for all three cases as we expected. Note that the concentrations at $\phi=0.1$, which we regarded as the composition of liquid at the interface in the preceding section, are very close to the maximum values in all cases.

We compared the solid and liquid compositions at the interface obtained in the numerical simulation with those predicted with low interface velocity limit condition. The solid and liquid compositions at the interface in numerical simulation were taken as the minimum and maximum values, respectively, in the concentration profiles given in Fig. 3. The solutions of Eqs. (33) and (34), c_S and c_L, were obtained by an iterative method on the compositions, using the free energy densities of solid and liquid phases given in Table I, where we used $\alpha=(2.552/M+0.3280)\times10^8$ J s/m^4 and $\beta=1.858\times10^9$ Js/m^4 which were obtained from Eqs. (37) and (38) for the same w, ϵ, and $D(\phi)$ as in the numerical simulation. In order to check the effects of phase-field mobility, two cases were considered; $M=44$ and $M=2.2$ m^3/J s were assumed and corresponding interface kinetics coefficients were 0.0165 m/K s and 0.0043 m/K s, respectively, which were calculated from Eq. (47) under the assumption of dilute solution.

Figures 4 and 5 show interface velocity dependencies of liquid and solid compositions at the interface, respectively. In these figures, solid circles ($M=44$ m^3/J s) and open circles ($M=2.2$ m^3/J s) are the results obtained by numerical simulation, and solid curves ($M=44$ m^3/J s) and dashed curves ($M=2.2$ m^3/J s) are those predicted at low interface velocity limit condition. As discussed in the preceding sec-

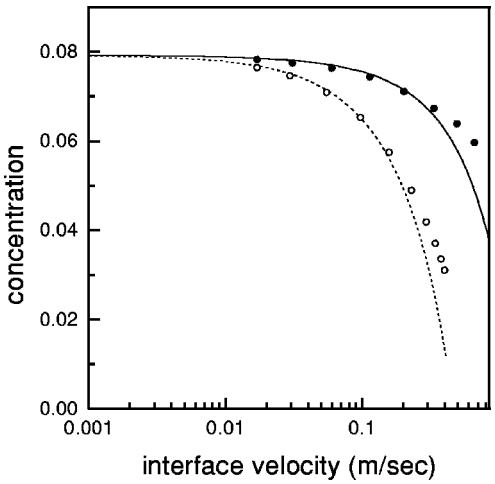

FIG. 4. Variations of the liquid concentration at the interface with the interface velocity. The solid ($M=44$ m^3/J s) and dashed curves ($M=2.2$ m^3/J s) are the predictions with low interface velocity limit condition, and the filled circles ($M=44$ m^3/J s) and open circles ($M=2.2$ m^3/J s) are the results obtained from numerical simulations with the same parameters.

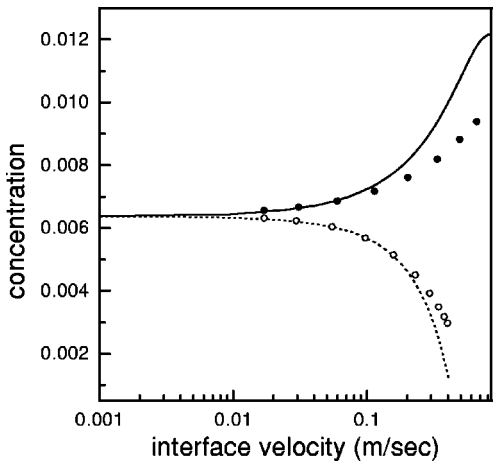

FIG. 5. Variations of the solid concentration at the interface with the interface velocity. The solid ($M=44$ m^3/J s) and dashed curves ($M=2.2$ m^3/J s) are the predictions with low interface velocity limit condition, and the filled circles ($M=44$ m^3/J s) and open circles ($M=2.2$ m^3/J s) are the results from numerical simulations with the same parameters.

tion, with a small M value both solid and liquid compositions decrease with the increasing interface velocity. When M is large, however, the solid composition increases and the solid and liquid concentrations approach each other. We can see the compositions predicted with low interface velocity limit condition are in good agreements with those from the numerical simulations, especially in the region of interface velocity less than 0.2 m/s.

VII. CONCLUSION

For the phase-field model for solidification of an alloy, we represented the relationship between the material properties and the parameters in the phase-field equation with the low interface velocity limit condition and with a finite interface thickness, not in the sharp interface limit. Finite interface thickness induced a chemical potential gradient within the diffuse interface and caused the compositions of solid and liquid at the interface to approach each other with increasing interface velocity, which is the solute trapping phenomenon. One-dimensional isothermal solidification of the Al–2-mole-%-Si alloy at 870 K was simulated by a numerical method. The interfacial compositions of solid and liquid predicted at a low interface velocity limit condition were in good agreement with those from the numerical simulations, especially in the region of interface velocity less than 0.2 m/s.

There exist upper bounds on the interface thickness and the interface kinetics coefficient which vary with thermophysical properties of alloys. The upper bound for the interface kinetics coefficient disappears only at sharp interface limit condition or infinite interfacial diffusivity condition. The calculated upper bound of interface thickness for the Al–2-mole-%-alloy at 870 K was 6.51 nm. The upper bound on the interface kinetics coefficient, calculated with an interface thickness of 3 nm, was 0.0195 m/s K. These upper bounds may impose strong restrictions on the numerical simulation of pattern formation during solidification with a reasonable interface kinetics coefficient ($\sim$1 m/s K) and a large system size. After submission of this paper, we learned that similar results were obtained independently by Ahmad [30].

[1] J. S. Langer, *Directions in Condensed Matter*, edited by G. Grinstein and G. Mazenko (World Scientific, Singapore, 1986), p. 164.
[2] G. Caginalp, Phys. Rev. A **39**, 5887 (1989).
[3] R. Kobayashi, Physica D **63**, 410 (1993).
[4] J. B. Collins and H. Levine, Phys. Rev. B **31**, 6119 (1985).
[5] G. B. McFadden, A. A. Wheeler, R. J. Braun, S. R. Coriell, and R. F. Sekerka, Phys. Rev. E **48**, 2016 (1993).
[6] A. A. Wheeler, B. T. Murray, and R. J. Schaefer, Physica D **66**, 243 (1993).
[7] S.-L. Wang and R. F. Sekerka, Phys. Rev. E **53**, 3760 (1996).
[8] O. Penrose and P. C. Pife, Physica D **43**, 44 (1990).
[9] S.-L. Wang, R. F. Sekerka, A. A. Wheeler, B. T. Murray, S. R. Coriell, R. J. Braun, and G. B. McFadden, Physica D **69**, 189 (1993).
[10] A. A. Wheeler, W. J. Boettinger, and G. B. McFadden, Phys. Rev. A **45**, 7424 (1992).
[11] G. Caginalp and W. Xie, Phys. Rev. E **48**, 1897 (1993).
[12] J. A. Warren and W. J. Boettinger, Acta Metall. Mater. **43**, 689 (1995).
[13] H. Löwen, J. Bechhoefer, and L. S. Tuckerman, Phys. Rev. A **45**, 2399 (1992).
[14] A. A. Wheeler, G. B. McFadden, and J. B. Boettinger, Proc. R. Soc. London, Ser. A **452**, 495 (1996).
[15] A. Karma, Phys. Rev. E **49**, 2245 (1994).
[16] K. R. Elder, F. Drolet, J. M. Kosterlitz, and M. Grant, Phys. Rev. Lett. **72**, 677 (1994).
[17] I. Steinbach, F. Pezzolla, B. Nestler, M. Seeßelberg, R. Prieler, G. J. Schmitz, and J. L. L. Rezenda, Physica D **94**, 135 (1996).
[18] B. Billia and R. Trivedi, in *Handbook of Crystal Growth 1, Part B*, edited by D. J. T. Hurle (North-Holland, Amsterdam, 1993), p. 1052.
[19] M. J. Aziz, J. Appl. Phys. **53**, 1158 (1982).
[20] M. J. Aziz and T. Kaplan, Acta Metall. **36**, 2335 (1988).
[21] A. A. Wheeler, W. J. Boettinger, and G. B. McFadden, Phys. Rev. E **47**, 1893 (1993).
[22] W. J. Boettinger, A. A. Wheeler, B. T. Murrary, and G. B. McFadden, Mater. Sci. Eng., A **178**, 217 (1994).
[23] M. Conti, Phys. Rev. E **55**, 701 (1997).
[24] M. Conti, Phys. Rev. E **55**, 765 (1997).
[25] A. A. Wheeler, N. A. Ahmad, W. J. Boettinger, R. J. Braun, G. B. McFadden, and B. T. Murray, Adv. Space Res. **16**, 163 (1995).
[26] A. Karma and W. J. Rappel, Phys. Rev. E **53**, R3017 (1996).
[27] J. L. Murrary and A. J. McAlister, Bull. Alloy Phase Diagrams **5**, 74 (1984).
[28] J. W. Christian, *Theory of Transformation in Metals and Alloys Part II* (Pergamon Press, Oxford, 1975).
[29] W. J. Boettinger and S. R. Coriell, in *Science and Technology of Undercooled Melts*, edited by P. R. Sahm, H. Johns, and C. M. Adam (Martinus Nijhoff, Dordrecht, 1986), p. 81.
[30] N. A. Ahmad, Ph.D. thesis, University of Southampton, 1997.